

Synthesized multiwall MoS₂ nanotube and nanoribbon field-effect transistors

S. Fathipour,^{1,a)} M. Remskar,² A. Varlec,² A. Ajoy,¹ R. Yan,³ S. Vishwanath,¹
W. S. Hwang,⁴ H. G. Xing,¹ D. Jena,¹ and A. Seabaugh^{1,b)}

¹ Department of Electrical Engineering, University of Notre Dame, Notre Dame, Indiana 46556, USA

² Solid State Physics Department, Jožef Stefan Institute, Ljubljana, Slovenia

³ Department of Electrical Engineering, Cornell University, Ithaca, New York 14850, USA

⁴ Department of Materials Engineering, Korea Aerospace University, Gyeonggi 412791, Korea

We report on the fabrication and characterization of synthesized multiwall MoS₂ nanotube (NT) and nanoribbon (NR) field-effect transistors (FETs). The MoS₂ NTs and NRs were grown by chemical transport, using iodine as a transport agent. Raman spectroscopy confirms the material as unambiguously MoS₂ in NT, NR, and flake forms. Transmission electron microscopy was used to observe cross sections of the devices after electrical measurements and these were used in the interpretation of the electrical measurements allowing estimation of the current density. The NT and NR FETs demonstrate *n*-type behavior, with ON/OFF current ratios exceeding 10³, and with current densities of 1.02 μA/μm, and 0.79 μA/μm at $V_{DS} = 0.3$ V and $V_{BG} = 1$ V, respectively. Photocurrent measurements conducted on a MoS₂ NT FET, revealed short-circuit photocurrent of tens of nanoamps under an excitation optical power of 78 μW and 488 nm wavelength, which corresponds to a responsivity of 460 μA/W. A long channel transistor model was used to model the common-source characteristics of MoS₂ NT and NR FETs and was shown to be consistent with the measured data.

^{a)} Electronic mail: sfathipo@nd.edu

^{b)} Electronic mail: seabaugh.1@nd.edu

There is a growing interest in atom-thick materials such as graphene and the transition metal dichalcogenides (TMDs) for electronics applications^{1,2}. Bulk and single layer sheets of TMDs are beginning to be explored in a wide range of optoelectronic and electronic devices including solar cells^{3,4}, photodetectors^{5,6}, sensors^{7,8}, field-effect transistors^{9,10,11,12}, and logic circuits^{13,14}. The absence of surface dangling bonds, the excellent gate electrostatics of the few-layer transistor, and the potential for large area planar processing are all motivating this research. While planar processing is desirable for manufacturing, at the limits of scaling, the properties of these materials may be compromised by unpassivated dangling bonds at the sheet edges. Edges introduce traps, which can degrade subthreshold swing and increase tunneling leakage, $1/f$ noise, and variability in the device characteristics. Edges can be substantially eliminated by using nanotubes (NTs), and nanoribbons (NRs) formed from collapsed NTs.

There are only a few experimental reports of TMD NT transistors and these are based on WS₂^{15,16} and MoS₂^{17,18}. Density functional theory shows that WS₂ and MoS₂ NTs are semiconducting with well-defined band gaps^{19,20}. Levi¹⁵ reported *n*-channel conduction on a 75 nm diameter WS₂ multiwall NTs with an ON/OFF current ratio of about 2; this commercial material was dispersed from powder. Unalan¹⁶ used multiwall NTs synthesized by conversion of tungsten oxide particles²¹; the ON/OFF current ratio was about 4. The first MoS₂ NT FET report by Remškar¹⁷ showed no gate modulation and no photoresponse on a multiwall NT with a diameter of approximately 100 nm and synthesized from Mo₆S₄I₆ nanowires by sulphurization using H₂S/ H₂/ Ar gas mixture, the method that causes a high density of structural defects²². In a recent report, Strojnik¹⁸ confirmed transistor action with *n*-channel conduction in MoS₂ NTs based on the same synthesis method and achieved an ON/OFF current ratio of 60. In this paper we report on the properties of MoS₂ NT and NR FETs in which an ON/OFF current ratio exceeding 10^3 is achieved.

The NTs used in this study were grown by chemical transport reaction, which enables growth of NTs with very slow rate from the vapor phase²³. The silica ampoule containing MoS₂ powder and iodine in amount of 1.5 mg/cm³ was evacuated and sealed at a pressure of 7×10^{-4} Pa. The transport reaction using iodine as a transport agent ran from 1133 K to 1010 K with a temperature gradient of 6.2 K/cm in a two-zone furnace. After three weeks of growth, the silica ampoules were cooled to room temperature with a controlled cooling rate of 60° C/hour. Approximately a few percent of the starting material was transported by the reaction to form nanotubes, while the rest of the transported material grows as strongly undulated thin plate-like crystals. The nearly equilibrium growth conditions enable the synthesis of nanotubes of different diameters, length, and wall thickness, but with extremely low density of structural defects. They grow up to several millimeters in length. The

diameters in multi-wall nanotubes range from several micrometers to less than ten nanometers. Some of the nanotubes spontaneously collapse during the growth and continue in growth in ribbon shapes²⁴.

The completed transistor planar views and schematic cross section are shown in Figure 1. The process flow consisted of electron-beam evaporation of Ti/Au (5/100 nm) on the back of the Si wafer. The MoS₂ nanostructures were exfoliated using 3M Scotch 810 tape onto 26 nm Al₂O₃ formed by atomic layer deposition. The NTs and NRs were then patterned to form the source and drain contacts using electron beam lithography followed by deposition of Sc/Ni (40 nm/ 20 nm) metal contacts. Figure 1 shows (a) scanning electron microscope (SEM) image, (b) atomic force microscope (AFM) image, and (c) schematic cross section of the FET.

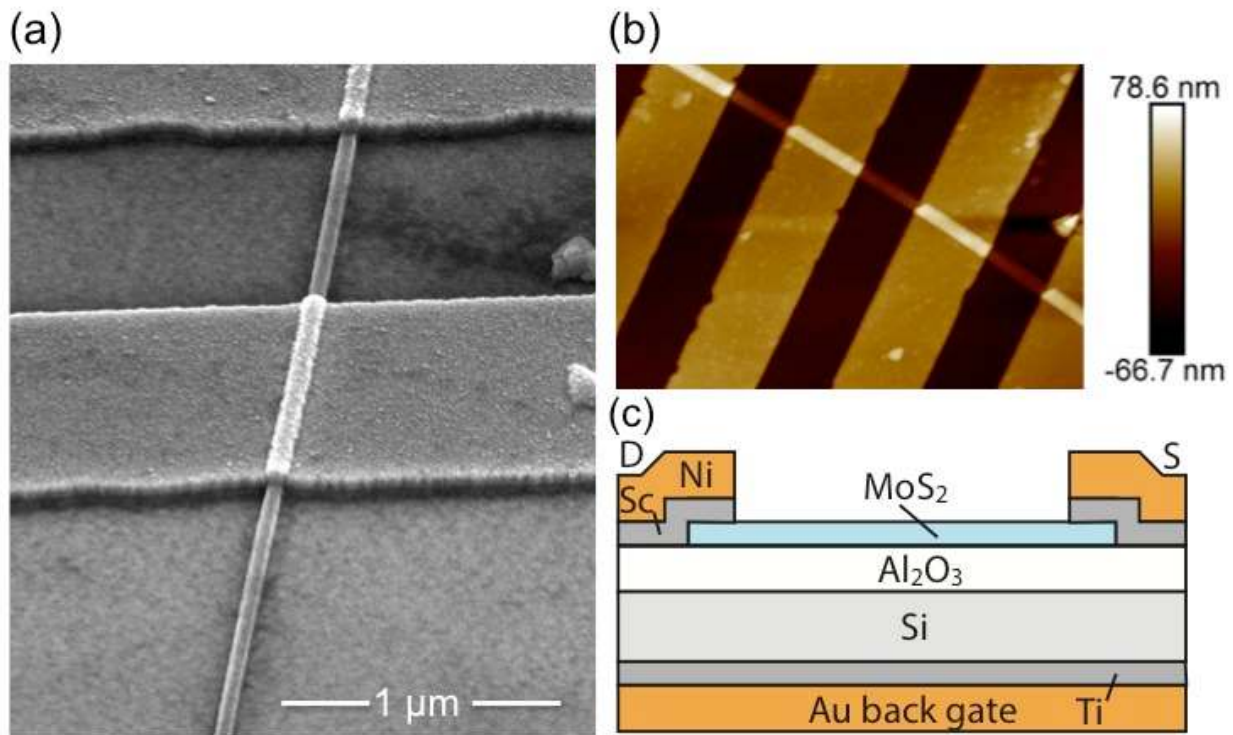


FIG. 1. (a) SEM image, (b) AFM image and (c) schematic cross-section of a MoS₂ NT FET. The four-contacts Kelvin connection shown in (b) was used to measure the contact resistance.

Transmission electron microscope (TEM) images were taken following the electrical measurements to establish clearly the cross section of the measured devices. Fig. 2, images (a) and (b) are of the NR and (c) shows the NT. Both nanostructures are multiwall and the ribbon is a collapsed nanotube with a total thickness of about 7 nm and 10 monolayers. This would give an interlayer distance of 0.7 nm for the NR. As shown by the TEM image of Fig. 2(c), NT has an elliptical shape with a wall thickness of 11 layers. Interlayer distance in NT based on the TEM results is 0.68 nm. The interlayer distance in both NR and

NT, is close to the range of 0.62 to 0.68, reported in literature^{25,26,27}. High-resolution TEM images, not shown, reveal that the MoS₂ has the 2H hexagonal structure.

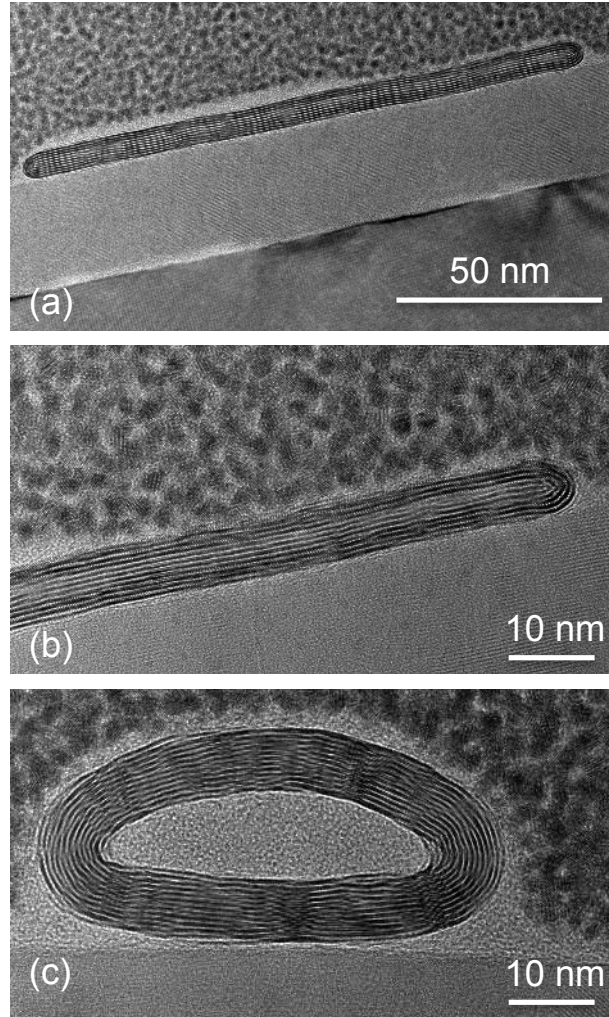


FIG. 2. Transmission electron microscope image of the transistor channel cross sections: (a) MoS₂ nanoribbon with width of 140 nm, height of 7 nm, and cross sectional area of 980 nm². The nanoribbon has a layer thickness of 10 monolayers. (b) MoS₂ nanoribbon magnified to show wrapping of the layers at the ribbon edge. (c) MoS₂ NT with a layer thickness of 11 monolayers and cross sectional area of 766 nm². The minor and major radii for the inner ellipse are 5 nm and 20 nm, respectively, and for the outer ellipse are 12.5 nm and 27.5 nm.

Raman measurements, shown in Fig. 3(a), were performed on the NR, the NT, and a flake that was exfoliated from the same material source. Measurements were done in the backscattering configuration using a WITec Alpha 300 system at room temperature (100× objective, 488 nm laser wavelength, 144 kW/cm² power density). Clear signals of Raman in-plane vibrational mode, E_{2g}^1 , and out-of-plane vibrational mode, A_{1g} , for MoS₂ are observed in all the grown nanostructures. A slight red shift is observed in the Raman peaks of the NT and NR structures relative to the flake. Local heating due to laser illumination is known to red shift both the E_{2g}^1 and A_{1g} peaks in bulk, and few-layered MoS₂ as well as in MoS₂

microtubes^{28,29}. The conduction of heat out of the NT may be expected to be less than the NR because of smaller contact area to the substrate. Thus, heat may be expected to red shift the NT more than the NR, which is what is observed.

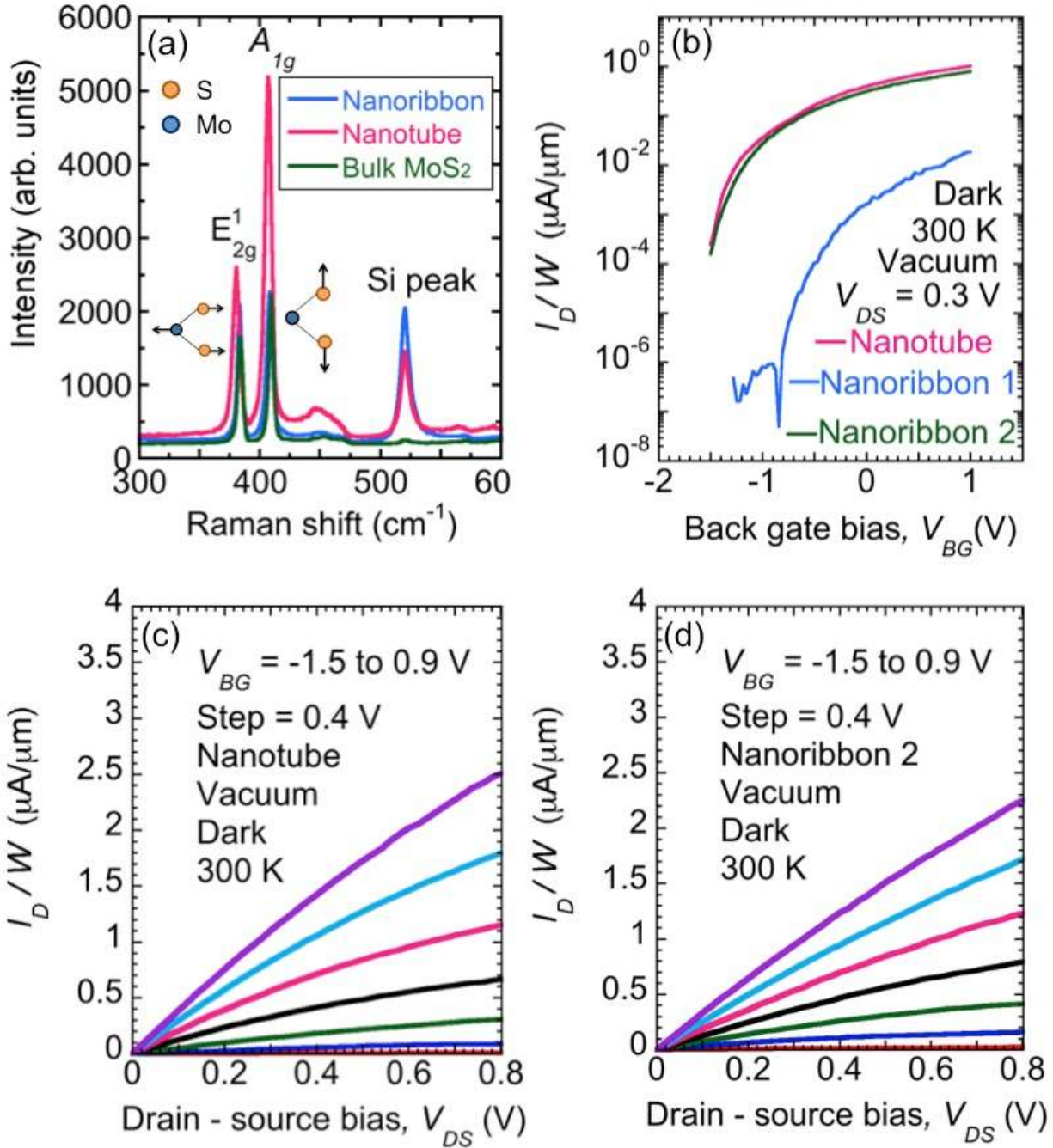


FIG. 3. (a) Raman spectrum of the MoS₂ NT, NR and bulk MoS₂ flake with a laser wavelength of 488 nm and power density of 144 kW/cm². The out-of-plane A_{1g} and in-plane E_{2g}¹ vibrations are identified in the inset. (b) Measured drain current per unit width vs. back-gate voltage for the MoS₂ NT FET and two MoS₂ NR FETs, designated NR1 and NR2. Channel widths are 55 nm, 140 nm, and 321 nm, respectively. (c) Common source characteristics for the MoS₂ NT FET measured in vacuum. (d) Common source characteristics for the MoS₂ NR2 FET measured in vacuum.

A smaller E_{2g}^1 over A_{1g} ratio was observed in the NT. This could be explained by the fact that in the back-scattering configuration, polarization of incoming light is perpendicular to the c-axis of the crystal in the NR, bulk MoS₂ and center of NT, while it is parallel to the c-axis at the edges of the NT. Direction of the A_{1g} mode vibration is parallel to the c-axis³⁰ and therefore its intensity increases at nanotube edges. The edges can contribute majority of the signal when diameter of NT is as small as tens of nanometers.

The measured drain current per unit width vs. back-gate voltage is shown in Fig. 3(b) for a NT and two NR FETs, designated NR1 and NR2. All transistors showed *n*-channel conduction, with ON/OFF current ratios of more than 10³. In the course of the measurement, the reverse bias was limited to -1.5 V, wherein the leakage current was less than a few pA. As a result, the value of 10³ for the NT and NR2 FET should be considered a lower limit. This value for the NT FET far exceeds the prior best report of 60 by Strojnik¹⁸. From the measured dimensions given in the caption of Fig. 2, the width for the NT and the NR1 can be estimated to be 55 nm and 140 nm. The measured width for NR2 is 321 nm. The corresponding values for the extracted current per unit width measured in NT, NR1 and NR2 FETs are 1.02 $\mu\text{A}/\mu\text{m}$, 0.02 $\mu\text{A}/\mu\text{m}$, and 0.79 $\mu\text{A}/\mu\text{m}$ at $V_{DS} = 0.3$ V and $V_{BG} = 1$ V. The lower current density in NR1 FET is not well explained by contacts or mobility and remains a question.

The electrical characteristics of the back-gated MoS₂ NT and NR2 FETs are further modeled using a long channel FET model. The detailed description of this model is included in the supplementary material³¹. Carrier density, mobility and flat band voltage are the unknowns in the model. Using a charge density of $1 \times 10^{16} \text{ cm}^{-3}$, mobility of 43.5 cm^2/Vs and flat band voltage of -0.9 V for the MoS₂ NT FET and a charge density of $1 \times 10^{16} \text{ cm}^{-3}$, mobility of 36 cm^2/Vs and flat band voltage of -1 V for the MoS₂ NR2 FET, an excellent fit to the experimental data was obtained, see supplemental material.

The sole report of MoS₂ NR FETs, by Liu³², utilized reactive ion etching to form ribbons as narrow as 60 nm from exfoliated flakes. Liu achieved an ON/OFF current ratio of nearly 10⁴ on *n*-channel FETs for a 60 nm NR width with a 6 nm thickness. This exceeds the 10³ ON/OFF ratio obtained here. Subthreshold swing is much improved in this paper, Our minimum subthreshold swing for both NR FETs is 200 mV/decade, compared to 10 V/decade in the MoS₂ NR FET by Liu³². The enhanced subthreshold swings in the NR can be attributed to two factors. Firstly, the NR in our FET is grown. Therefore, edge roughness and defects due to dangling bonds are largely nonexistent. This is in contrast with the NRs formed by plasma

dry etching of MoS₂ flakes by Liu. Secondly, to fabricate devices, we use 26 nm of Al₂O₃, whereas Liu uses 300 nm SiO₂. This will extend the SS by factor of 10×, bringing the two results more closely in line.

Four point probe measurements were used to extract the contact resistance of the MoS₂ NT FET with a Sc contact. The extracted value for contact resistance at $V_{BG} = 0$ V was 39.6 kΩ.μm. This exceeds the reported value of 10 kΩ.μm by Das in [33] for same overdrive voltage and with same contact on MoS₂. As outlined by Das³³, the extracted resistance involves contributions from both Schottky barrier resistance and also resistive coupling between the layers of the 2D material. Therefore, the resistance due to the Schottky barriers may be less than this value.

Scanning photocurrent measurements were also conducted on MoS₂ NT FETs, fabricated with Ti/ Au (1 nm/100 nm) source and drain contacts on a highly-doped Si wafer covered by 285 nm SiO₂. A WITec Alpha 300 scanning confocal microscope was used to focus a 488 nm wavelength laser onto the NT FET. The beam diameter was determined to be about 660 nm. Using spot area and the measured laser power, a power density of 22 kW/cm² was determined. Photocurrent was recorded as the laser spatially scanned the sample. Current was converted to a voltage using a transimpedance amplifier. The reflected light was simultaneously collected to correlate with the spatial photocurrent mapping. Fig. 4(a), shows a representative short-circuit photocurrent ($V_{DS} = V_{BG} = 0$) mapping of a MoS₂ NT FET, with the metal 1 as drain, metal 2 floating, and metal 3 as source. Fig. 4 (b) shows the photocurrent profile along the blue dotted line of Fig. 4(a). Prominent negative and positive photocurrents are detected at the drain and source side, respectively. The photocurrent is due to the separation of photogenerated carriers by band bending at the metal-semiconductor junctions, which dominate the voltage drop in the TMD FET. Responsivity is defined as the ratio of photocurrent, divided by the incident power on the nanotube. The incident power on the nanotube was found by multiplying the total power of the laser and the area ratio of the nanotube and laser spot. The responsivity is ~ 460 μA/W close to that of graphene reported in [34].

Using the Schottky photocurrent mapping of Fig. 4(b), we estimate the band bending profile near source/ MoS₂ junction and drain/ MoS₂ junction. When the NT is illuminated near the drain or source contact, electron/ hole pairs are locally generated at the illumination region. Under the built in Schottky field at NT/metal junction, the electron and the hole are separated with the current direction set by the band bending. To match the observed photocurrent polarity, the bands are bent upward, as indicated in the band diagram shown in the inset of Fig. 4(b).

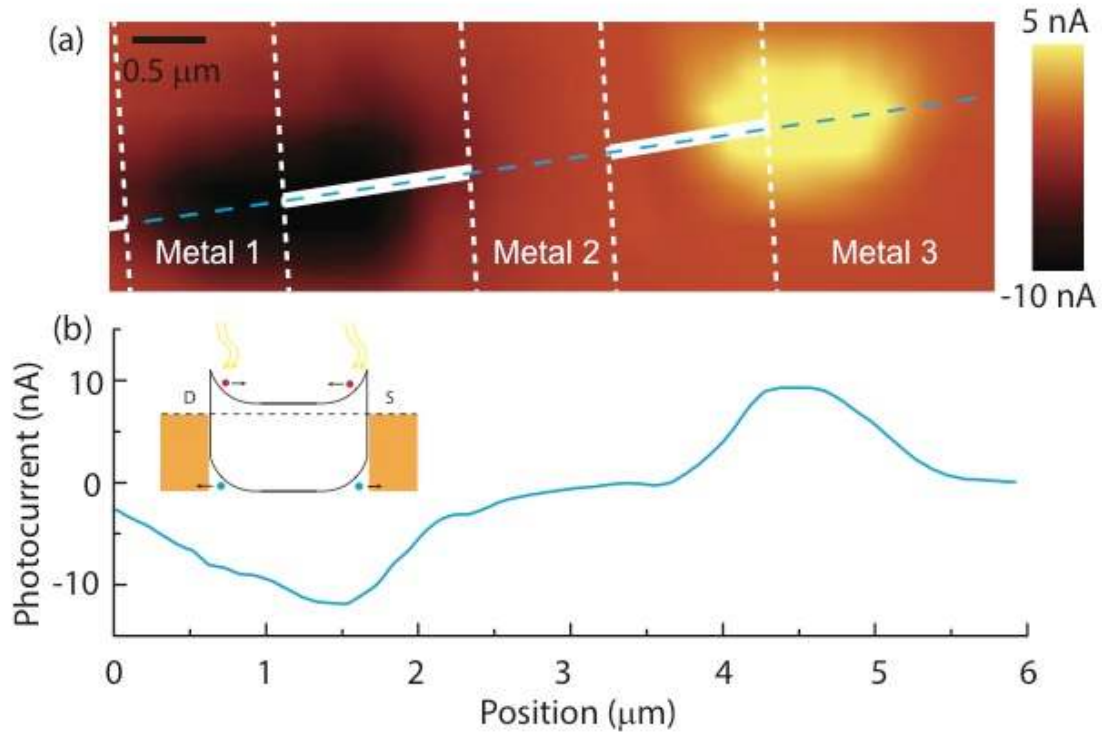


FIG. 4. (a) Representative short-circuit photocurrent mapping of a MoS₂ NT FET. (b) The line profile is the photocurrent along the dotted blue line in (a). The inset shows the schematic of the band bending in the MoS₂ NT device. Blue and red carriers refer to holes and electrons, respectively.

In conclusion, synthesized MoS₂ NT and NR FETs were fabricated and characterized. Devices demonstrated *n*-type characteristics with ON/OFF current ratios of more than 10³, greatly exceeding the best prior report of 60 in the NT case. Raman measurements confirm the E_{2g}¹ and A_{1g} vibrational modes in both tubes and ribbons with a red shift compared to bulk MoS₂, due to laser heating effect. Photocurrent measurements were conducted on MoS₂ NT FET with Ti/ Au contacts and revealed a responsivity of ~ 460 μA/W. The common-source characteristics were shown to be in good agreement with a long channel transistor model.

ACKNOWLEDGMENTS

This work was supported in part by the Center for Low Energy Systems Technology (LEAST), a STARnet Semiconductor Research Corporation program sponsored by MARCO and DARPA.

REFERENCES

- 1 D. Jena, Proc. IEEE 101, 1585 (2013).
- 2 G. Fiori, F. Bonaccorso, G. Iannaccone, T. Palacios, D. Neumaier, A. Seabaugh, S. K. Banerjee, and L. Colombo, Nature Nanotech. 9, 768 (2014).
- 3 M.L. Tsai, S. H Su, J.K. Chang, D.S. Tsai, C.H. Chen, C.I. Wu, L. J. Li, L. J. Chen, and J. H. He, ACS Nano 8, 8317 (2014).
- 4 G Prasad and O N Srivastava, J. Phys. D: Appl. Phys. 21, 1028 (1988).
- 5 O. L. Sanchez, D. Lembke, M. Kayci, A. Radenovic, and A. Kis, Nature Nanotech. 8, 497 (2013).
- 6 B. Baugher, H. Churchill, Y. Yang, and P. Herrero, Nature Nanotech. 9, 262 (2014).
- 7 D. J. Late, Y. K. Huang, B. Liu, J. Acharya, S. N. Shirodkar, J. Luo, A. Yan, D. Charles, U. V. Waghmare, V. P. Dravid, and C. N. R. Rao, ACS Nano 7, 4879 (2013).
- 8 F. K. Perkins, A. L. Friedman, E. Cobas, P. M. Campbell, G. G. Jernigan, and B. T. Jonker, Nano Lett. 13, 668 (2013).
- 9 B. Radisavljevic, A. Radenovic, J. Brivio, V. Giacometti, and A. Kis, Nature Nanotech. 6, 147 (2011).
- 10 S. Fathipour, W. S. Hwang, T. H. Kosel, H. Xing, W. Haensch, D. Jena and A. C. Seabaugh, 2013 Dev. Res. Conf. (DRC), 115-116.
- 11 S. Fathipour, N. Ma, W. S. Hwang, V. Protasenko, S. Vishwanath, H. G. Xing, H. Xu, D. Jena, J. Appenzeller, and A. Seabaugh, Appl. Phys. Lett. 105, 192101 (2014).
- 12 W. S. Hwang, M. Remskar, and R. Yan, Appl. Phys. Lett. 101, 013107 (2012).
- 13 M. Tosun, S. Chuang, H. Fang, A. B. Sachid, M. Hettick, Y. Lin, Y. Zeng, and Ali Javey, ACS Nano 8, 4948 (2014).
- 14 Branimir Radisavljevic, Michael B. Whitwick, and Andras Kis, ACS Nano 7, 3729 (2013).
- 15 R. Levi, O. Bitton, G. Leitner, R. Tenne, and E. Joselevich, Nano Lett. 13, 3736 (2013).
- 16 H. E. Unalan, Y. Yang, Y. Zhang, P. Hiralal, D. Kuo, S. Dalal, T. Butler, S. N. Cha, J. E. Jang, K. Chremmou, G. Lentaris, D. Wei, R. Rosentsveig, K. Suzuki, H. Matsumoto, M. Minagawa, Y. Hayashi, M. Chhowalla, A. Tanioka, W. I. Milne, R. Tenne, and G. A. J. Amaratunga, IEEE Trans. Electron Dev. 55, 2988 (2008).
- 17 M. Remškar, A. Mrzel, M. Virsek, M. Godec, M. Krause, A. Kolitsch, A. Singh, and A. Seabaugh, Nanoscale Res. Lett. 6, 26 (2011).
- 18 M. Strojnik, A. Kovic, A. Mrzel, J. Buh, J. Strle, D. Mihailovic, AIP Advances 4, 097114 (2014).
- 19 G. Seifert, H. Terrones, M. Terrones, G. Jungnickel, and T. Frauenheim, Phys. Rev. Lett. 85, 146 (2000).
- 20 G. Seifert, H. Terrones, M. Terrones, G. Jungnickel, T. Frauenheim, Solid State Comm. 114, 245 (2000).
- 21 A. Rothschild, J. Sloan, and R. Tenne, J. Am. Chem. Soc. 122, 5169 (2000).
- 22 M. Virsek, N. Novak, C. Filipic, P. Kump, M. Remskar, Z. Kutnjak, J. Appl. Phys. 112, 103710-1 (2012).
- 23 M. Remskar, Z. Skraba, M. regula, C. Ballif, R. Sanjines, F. Levy, Adv. Mater. 10, 246 (1998).
- 24 M. Remskar, Z. Skraba, F. Cleton, R. Sanjines, F. Levy, Surface Rev. Lett. 5, 423 (1998)
- 25 X. Zhang, W. P. Han, J. B. Wu, S. Milana, Y. Lu, Q. Q. Li, A. C. Ferrari, and P. H. Tan, Phys. Rev. B 87, 115413 (2013).
- 26 Y. Zhan, Z. Liu, S. Najmaei, P. M. Ajayan, and J. Lou, Small 8, 966, (2012).
- 27 P. D. Fleischauer, R. Jeffrey, P. Lince, A. Bertrand and R. Bauer, Langmuir 5, 1009 (1989).
- 28 M. Viršek, M. Krause, A. Kolitsch, and M. Remškar, Phys. Stat. Solidi (b) 246, 2782 (2009).
- 29 S. Najmaei, Z. Liu, P. M. Ajayan and J. Lou, Appl. Phys. Lett. 100, 013106 (2012).
- 30 T.J. Wieting and J. L. Verble, Phys. Rev. B 3, 4286 (1971).
- 31 See supplementary material at [URL will be inserted by AIP] for details on our analytical model.
- 32 H. Liu, J. Gu, and P. Ye, IEEE Electron Dev. Lett. 33, 1273 (2012).
- 33 S. Das and J. Appenzeller, Nano Lett. 13, 3396 (2013).
- 34 F. Xia, T. Mueller, Y. Lin, A. V. Garcia, and P. Avouris, Nature Nanotech. 4, 839 (2009).

Supplemental Material

Synthesized multiwall MoS₂ nanotube and nanoribbon field-effect transistors

S. Fathipour¹, M. Remskar², A. Varlec², A. Ajoy^{1,a}, R. Yan³, S. Vishwanath¹, W. S. Hwang⁴, H. G. Xing¹, D. Jena^{1,b}, and A. Seabaugh¹

¹ Department of Electrical Engineering, University of Notre Dame, Notre Dame, Indiana 46556, USA

² Solid State Physics Department, Jožef Stefan Institute, Ljubljana, Slovenia

³ Department of Electrical Engineering, Cornell University, Ithaca, New York 14850, USA

⁴ Department of Materials Engineering, Korea Aerospace University, Gyeonggi 412791, Korea

a) aajoy@nd.edu

b) djena@nd.edu

In this supplemental material, we attempt to model the current-voltage characteristics of the MoS₂ nanotube (NT) and nanoribbon (NR) MOSFETs. The growth of the NTs and NRs results in the MoS₂ being unintentionally *n*-doped. The fabricated *n*-type MOSFETs are hence accumulation-depletion devices – the channel is accumulated when the device is in the on-state, and is depleted of carriers as the device turns off. In accumulation, the channel is dominated by electrons that are close to the oxide-semiconductor interface. As the device turns off, the channel is dominated by electrons that are farther away from this interface. We restrict ourselves to gate voltages for which the channel is accumulated. In this regime, it is hence reasonable to approximate the cross section of the NT MOSFETs by a rectangle, as shown in Fig. S1. The thickness of this rectangle corresponds to the thickness of the wall of the NT. This approximation allows us to apply results derived for an *n*-type junctionless FET [1] to model both the NT and NR MOSFETs.

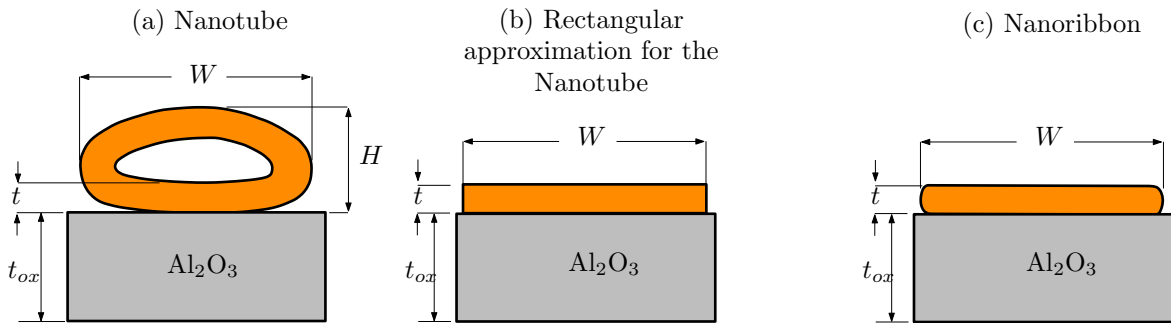


Figure S1: (a), (c) Cross-sections of the NT/NR MOSFETs along their width, and a rectangular approximation for the NT (b). This approximation is reasonable when the channel is strongly accumulated, since the channel lies close to the oxide-semiconductor interface in this regime of operation.

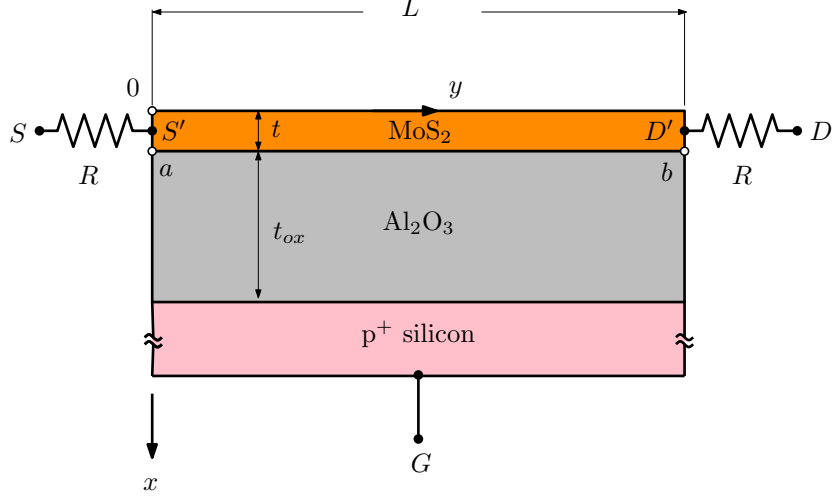


Figure S2: Cross-section of the approximate NT (Fig. S1(b)) and NR (Fig. S1(c)) devices along their length.

1 Model

See Fig. S2. S , D and G refer to the external terminals of the MOSFET. Source and drain contact resistances (assumed equal, R) connect S , D to intrinsic nodes S' and D' respectively. When a current I_D flows through the device, the terminal and intrinsic voltages are given by $V_{GS'} = V_{GS} - I_D R$, $V_{D'S'} = V_{DS} - 2I_D R$. Within the intrinsic MOSFET, the electron concentration is $n(x, y) = N_D \exp((\phi(x, y) - V(y))/V_t)$, where $\phi(x, y)$ is the quasi-Fermi potential, $V(y)$ is the electrostatic potential [2, 3], N_D is the unintentional doping concentration, and V_t is the thermal voltage. The surface potential $\phi_s(y) \equiv \phi(t, y)$ at the oxide-semiconductor interface is obtained by a solution of the following implicit equation

$$(V_{GS'} - V_{FB} - \phi_s)^2 = \frac{2\epsilon_s q N_D V_t}{C_{ox}^2} \left[\exp\left(\frac{\phi_s - V}{V_t}\right) - 1 \right] \quad (\text{S1})$$

where V_{FB} is the flat-band voltage, ϵ_s is the dielectric constant of MoS₂ and $C_{ox} = \epsilon_{ox}/t_{ox}$ with ϵ_{ox} , t_{ox} being the dielectric constant and thickness of the Al₂O₃ respectively. Note that this equation has been derived under the condition that the net charge density at the rear interface ($x = 0$) is zero in accumulation (which corresponds to $\phi(0, y) = V(y)$). Setting $V(0) = 0$ and $V(L) = V_{D'S'}$ in eq. (S1) respectively yields the surface potentials ϕ_a and ϕ_b (corresponding to the points a, b shown in Fig. S2). The current is then

$$I_D = \mu C_{ox} \frac{W}{L} \left[2V_t \phi_s + 2V_t \sqrt{\beta V_t} \arctan\left(\frac{V_{GS'} - V_{FB} - \phi_s}{\sqrt{\beta V_t}}\right) - \frac{1}{2}(V_{GS'} - V_{FB} - \phi_s)^2 \right]_{\phi_a}^{\phi_b} + \mu \frac{W}{L} q N_D t V_{D'S'} \quad (\text{S2})$$

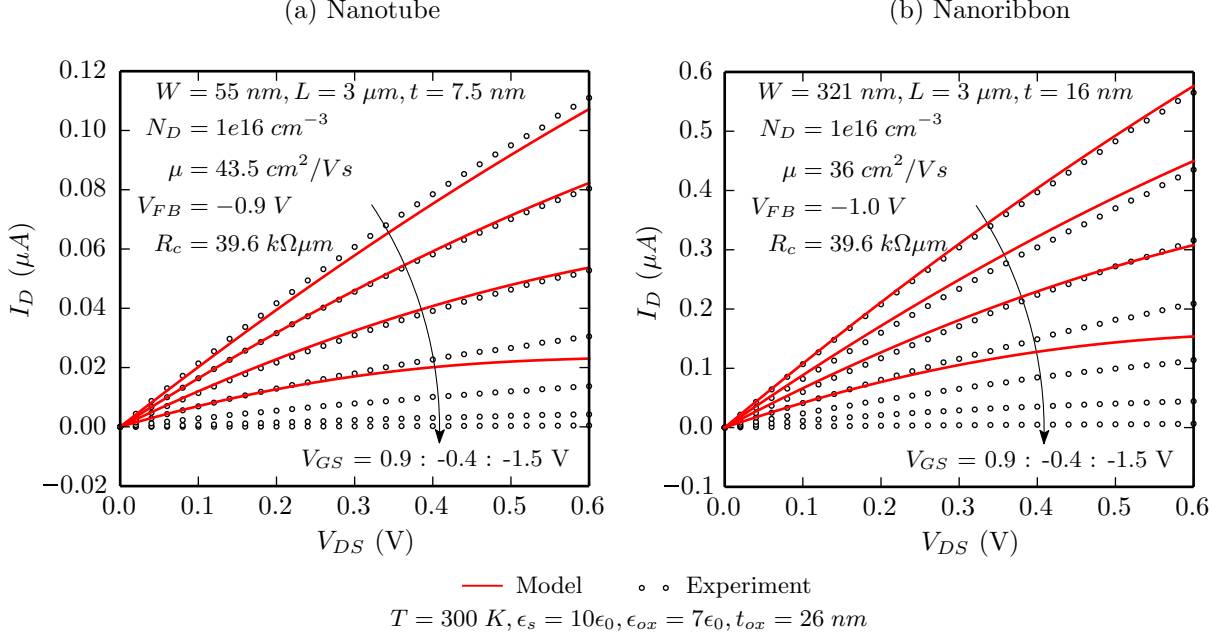


Figure S3: Comparison of experimental data with results from the model for the (a) nanotube and (b) nanoribbon MOSFETs. Parameter values used for the simulation are also shown. W, L, t, t_{ox}, T for the NT and NR, $R_c = R \cdot W$ for the NT are measured values. We have used the same value of R_c for the NR too. Values of ϵ_s and ϵ_{ox} are taken from [4]. Other parameters have been obtained by fitting the data to the model.

where μ is an effective value of mobility, and $\beta = 2\epsilon_s q N_D / C_{ox}^2$. A comparison of the experimental data with the results of the above model is shown in Fig. S3.

2 Verification of zero charge density approximation

We verify whether the approximation of zero net charge density at $x = 0$ is valid for the I_D - V_D curves we have modeled. To do this, we solve the electrostatic problem *without* this approximation, in terms of the surface potential ϕ_s and surface electric field E_s obtained using the zero charge density approximation. This allows us to plot the charge density $\rho(x)$ as a function of x . Our approximation is reasonable if $\rho(0)$ so obtained is close to zero. We begin with Poisson's equation under the gradual channel approximation given by

$$\frac{d^2\phi}{dx^2} = \frac{-\rho}{\epsilon_s} = \frac{qN_D}{\epsilon_s} \left(\exp\left(\frac{\phi - V}{V_t}\right) - 1 \right) \quad (\text{S3})$$

Integrating eq. (S3) by parts, we get $\int d(E^2) = -2 \int (\rho(\phi)/\epsilon_s) d\phi$ (where the electric field $E = -d\phi/dx$), which yields

$$E = -\sqrt{E_s^2 - \frac{2qN_D V_t}{\epsilon_s} \left[\exp\left(\frac{\phi_s - V}{V_t}\right) - \exp\left(\frac{\phi - V}{V_t}\right) - \exp\left(\frac{\phi_s - \phi}{V_t}\right) \right]} \quad (\text{S4})$$

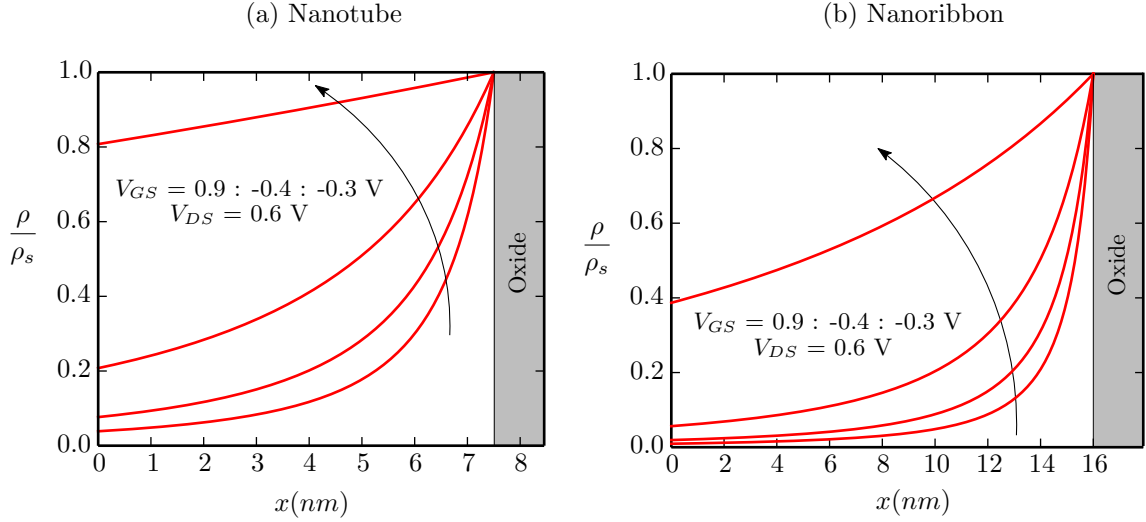


Figure S4: Verification of the approximation that charge density at the rear interface $\rho(0) = 0$ using a solution of eq. (S4) for the (a) nanotube and (b) nanoribbon mosfets. ρ_s is the charge density at the MoS₂-oxide interface ($x = t$). Notice that the difference between the model and experimental data in Fig. S3 is largest where the approximation $\rho(0) = 0$ is the worst.

The negative sign for the square root is sensible in the accumulation regime. Eq. (S4) can be cast as an ordinary differential equation $d\phi/dx' = f(\phi)$, with $x' = t - x$, and can be solved numerically to obtain $\phi(x)$ and $\rho(x)$, given the values of E_s, ϕ_s (which were obtained from a solution of eq. (S1)). The results from this calculation are shown in Fig. S4. The value of V in eq. (S4) is chosen to be equal to $\max(V_{D'S'})$. Notice that the approximation $\rho(0) \approx 0$ is the best for the largest value of V_{GS} , and worst for the lowest value of V_{DS} . This corresponds to the trends seen in Fig. S3.

3 Projection assuming ideal contacts

The minimum contact resistance to a 2-D material is given by $R_{c\ min} = 0.026/\sqrt{n_s} \text{ k}\Omega\mu\text{m}$, where n_s is the sheet charge density in units of $1e13 \text{ cm}^{-2}$ [5]. Assuming that $n_s = 1$ in the above expression, the minimum contact resistance is $R_{c\ min} = 0.026 \text{ k}\Omega\mu\text{m}$. Note that the value of contact resistance measured in our NT MOSFET is $R_c = 39.6 \text{ k}\Omega\mu\text{m}$. Fig. S5 predicts the currents that can be obtained from our NT and NR MOSFETs, provided the contact resistance is chosen to be $R_{c\ min}$. Improving the contacts in this manner causes a $\sim 27\%$ ($\sim 36\%$) increase in the currents of the NT (NR) at $V_{DS} = 0.6V$.

4 Conclusion

In conclusion, we have modeled the $I_D - V_D$ characteristics of the fabricated NT and NR MOSFETs operating in a regime where the entire channel is accumulated. The results of this model compare well with the experimental data. We extract effective mobilities of $43.5 \text{ cm}^2/Vs$ and $36 \text{ cm}^2/Vs$ for the NT and NR MOSFETs respectively.

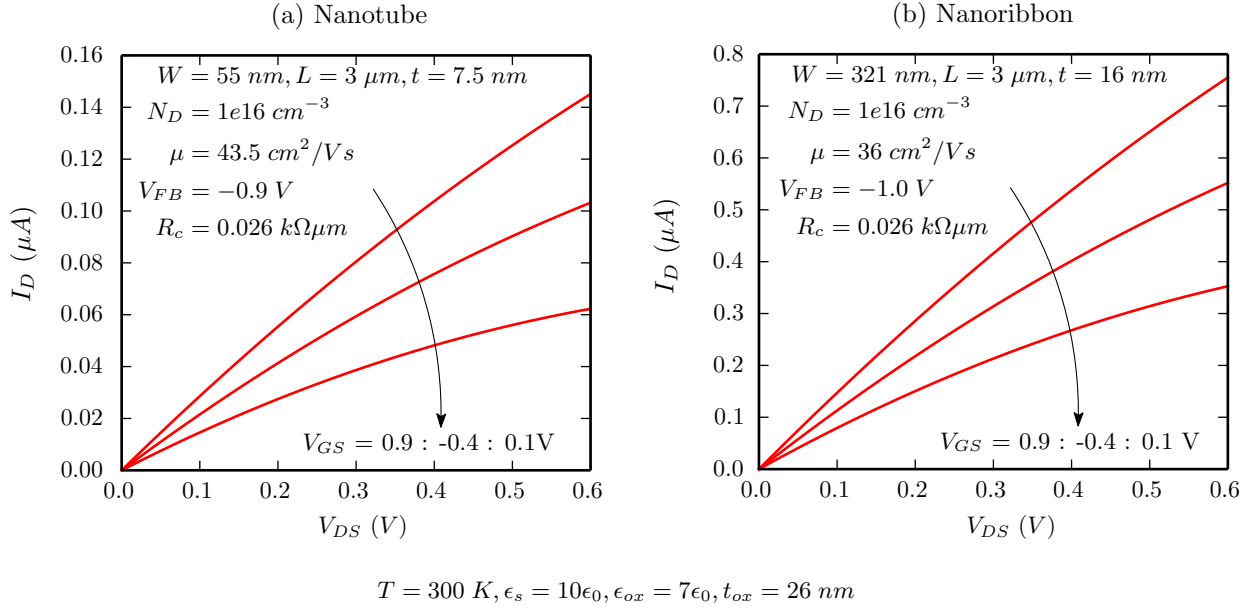


Figure S5: Projected $I_D - V_{DS}$ characteristics of the NT and NR MOSFETs assuming contact resistance $R_c = R_{c \text{ min}} = 0.026 \text{ k}\Omega\mu\text{m}$. Other parameters are identical to those in Fig. S3. An improvement of $\sim 27\%$ ($\sim 36\%$) is seen in the current at $V_{DS} = 0.6 \text{ V}$ for the NT (NR) as compared to Fig. S3.

References

- [1] Z. Chen, Y. Xiao, M. Tang, Y. Xiong, J. Huang, J. Li, X. Gu, and Y. Zhou, "Surface-potential-based drain current model for long-channel junctionless double-gate mosfets," *IEEE Trans. Electron Devices*, vol. 59, no. 12, pp. 3292–3298, 2012.
- [2] H. C. Pao and C.-T. Sah, "Effects of diffusion current on characteristics of metal-oxide (insulator)-semiconductor transistors," *Solid State Electron.*, vol. 9, no. 10, pp. 927–937, 1966.
- [3] A. Ortiz-Conde, R. Herrera, P. Schmidt, F. Sánchez, and J. Andrian, "Long-channel silicon-on-insulator MOSFET theory," *Solid State Electron.*, vol. 35, no. 9, pp. 1291–1298, 1992.
- [4] S. Kim, A. Konar, W.-S. Hwang, J. H. Lee, J. Lee, J. Yang, C. Jung, H. Kim, J.-B. Yoo, J.-Y. Choi *et al.*, "High-mobility and low-power thin-film transistors based on multilayer MoS_2 crystals," *Nature Communications*, vol. 3, p. 1011, 2012.
- [5] D. Jena, K. B. Banerjee, and G. H. Xing, "Intimate contacts," (*to appear*) *Nature Materials*.